

Shining Light on Dinitrogen Cleavage: Structural Features, Redox Chemistry, and Photochemistry of the Key Intermediate Bridging Dinitrogen Complex

John J. Curley, Timothy R. Cook, Steven Y. Reece, Peter Müller, and Christopher C. Cummins*

Department of Chemistry, Massachusetts Institute of Technology, 77 Massachusetts Avenue, Room 6-325, Cambridge, Massachusetts 02139

Received January 11, 2008; E-mail: ccummins@mit.edu

Abstract: The key intermediate in dinitrogen cleavage by $\text{Mo}(\text{N}[\textit{t}\text{-Bu}]\text{Ar})_3$, **1** ($\text{Ar} = 3,5\text{-C}_6\text{H}_3\text{Me}_2$), has been characterized by a pair of single crystal X-ray structures. For the first time, the X-ray crystal structure of $(\mu\text{-N}_2)[\text{Mo}(\text{N}[\textit{t}\text{-Bu}]\text{Ar})_3]_2$, **2**, and the product of homolytic fragmentation of the N–N bond, $\text{N}\equiv\text{Mo}(\text{N}[\textit{t}\text{-Bu}]\text{Ar})_3$, are reported. The structural features of **2** are compared with previously reported EXAFS data. Moreover, contrasts are drawn between theoretical predictions concerning the structural and magnetic properties of **2** and those reported herein. In particular, it is shown that **2** exists as a triplet ($S = 1$) at 20 °C. Further insight into the bonding across the MoNNMo core of the molecule is obtained by the synthesis and structural characterization of the one- and two-electron oxidized congeners, $(\mu\text{-N}_2)[\text{Mo}(\text{N}[\textit{t}\text{-Bu}]\text{Ar})_3]_2[\text{B}(\text{Ar}^{\text{F}})_4]$, $2[\text{B}(\text{Ar}^{\text{F}})_4]$ ($\text{Ar}^{\text{F}} = 3,5\text{-C}_6\text{H}_3(\text{CF}_3)_2$) and $(\mu\text{-N}_2)[\text{Mo}(\text{N}[\textit{t}\text{-Bu}]\text{Ar})_3]_2[\text{B}(\text{Ar}^{\text{F}})_4]_2$, $2[\text{B}(\text{Ar}^{\text{F}})_4]_2$, respectively. Bonding in these three molecules is discussed in view of X-ray crystallography, Raman spectroscopy, electronic absorption spectroscopy, and density functional theory. Combining X-ray crystallography data with Raman spectroscopy studies allows the N–N bond polarization energy and N–N internuclear distance to be correlated in three states of charge across the MoNNMo core. For $2[\text{B}(\text{Ar}^{\text{F}})_4]$, bonding is symmetric about the $\mu\text{-N}_2$ ligand and the N–N polarization is Raman active; therefore, $2[\text{B}(\text{Ar}^{\text{F}})_4]$ meets the criteria of a Robin–Day class III mixed-valent compound. The redox couples that interrelate **2**, **2**⁺, and **2**²⁺ are studied by cyclic voltammetry and spectroelectrochemistry. Insights into the electronic structure of **2** led to the discovery of a photochemical reaction that forms $\text{N}\equiv\text{Mo}(\text{N}[\textit{t}\text{-Bu}]\text{Ar})_3$ and $\text{Mo}(\text{N}[\textit{t}\text{-Bu}]\text{Ar})_3$ through competing N–N bond cleavage and N_2 extrusion reaction pathways. The primary quantum yield was determined to be $\Phi_p = 0.05$, and transient absorption experiments show that the photochemical reaction is complete in less than 10 ns.

Introduction

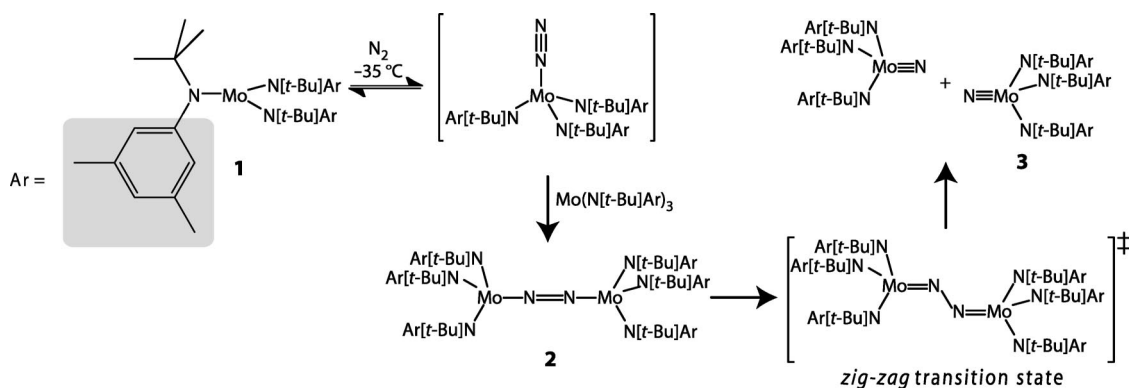
An outstanding goal in synthetic chemistry is the use of N_2 as a synthon for nitrogen-containing functional groups in organic molecules.^{1–5} In this regard, several procedures have been developed to transfer a nitrogen atom from an N_2 -derived metal nitride to an organic functional group.^{6–9} Limiting the development of new nitrogen transfer reactions is the small number of well-defined, transition-metal reagents that bind N_2 , form a $\mu\text{-N}_2$ complex, and subsequently cleave the N–N bond to form 2 equiv of a terminal nitride.^{10,11} While it is true that a large number of linear, bimetallic $\mu\text{-N}_2$ complexes have been isolated

and structurally characterized,^{7,12–25} these complexes typically require harsh conditions to promote reactions that productively use the N_2 fragment.¹⁵ This situation is unfortunate because linear $\mu\text{-N}_2$ complexes store N_2 in a reduced form and therefore should be susceptible to productive chemistry of the N_2 fragment.^{1,2} In contrast to linear $\mu\text{-N}_2$ complexes, bimetallic complexes that contain a side-bound $\mu\text{-N}_2$ ligand show enhanced

- (1) Chatt, J. *Philos. Trans. R. Soc. London, Ser. B* **1977**, *281*, 243–248.
- (2) MacKay, B. A.; Fryzuk, M. D. *Chem. Rev.* **2004**, *104*, 385–401.
- (3) Hidai, M.; Mizobe, Y. *Can. J. Chem.* **2005**, *83*, 358–374.
- (4) Hori, K.; Mori, M. *J. Am. Chem. Soc.* **1998**, *120*, 7651–7652.
- (5) Hori, M.; Mori, M. *J. Org. Chem.* **1995**, *60*, 1480–1481.
- (6) Curley, J. J.; Sceats, E. L.; Cummins, C. C. *J. Am. Chem. Soc.* **2006**, *128*, 14036–14037.
- (7) Figueroa, J. S.; Piro, N. A.; Clough, C. R.; Cummins, C. C. *J. Am. Chem. Soc.* **2006**, *128*, 940–950.
- (8) Watanabe, D.; Gondo, S.; Seino, H.; Mizobe, Y. *Organometallics* **2007**, *26*, 4909–4920.
- (9) Henderickx, H.; Kwakkenbos, G.; Peters, A.; van der Spoel, J.; de Vries, K. *Chem. Commun.* **2003**, 2050–2051.

- (10) Laplaza, C. E.; Johnson, M. J. A.; Peters, J. C.; Odom, A. L.; Kim, E.; Cummins, C. C.; George, G. N.; Pickering, I. J. *J. Am. Chem. Soc.* **1996**, *118*, 8623–8638.
- (11) Laplaza, C. E.; Cummins, C. C. *Science* **1995**, *268*, 861–863.
- (12) Manriquez, J. M.; Bercaw, J. E. *J. Am. Chem. Soc.* **1974**, *96*, 6229–6230.
- (13) Roddick, D. M.; Fryzuk, M. D.; Seidler, P. F.; Hillhouse, G. L.; Bercaw, J. E. *Organometallics* **1985**, *4*, 97–104.
- (14) Sanner, R. D.; Duggan, D. M.; McKenzie, T. C.; Marsh, R. E.; Bercaw, J. E. *J. Am. Chem. Soc.* **1976**, *98*, 8358–8365.
- (15) Schrock, R. R. *Acc. Chem. Res.* **2005**, *38*, 955–962.
- (16) Peters, J. C.; Cherry, J.-P. F.; Thomas, J. C.; Baraldo, L.; Mindiola, D. J.; Davis, W. M.; Cummins, C. C. *J. Am. Chem. Soc.* **1999**, *121*, 10053–10067.
- (17) Mindiola, D. J.; Meyer, K.; Cherry, J.-P. F.; Baker, T. A.; Cummins, C. C. *Organometallics* **2000**, *19*, 1622–1624.
- (18) Chatt, J.; Dilworth, J. R.; Richards, R. L. *Chem. Rev.* **1978**, *78*, 589–625.
- (19) Vidyaratne, I.; Scott, J.; Gambarotta, S.; Budzelaar, P. H. M. *Inorg. Chem.* **2007**, *46*, 7040–7049.

Scheme 1



reactivity,²⁶ and engage in productive reactions to liberate NH_3 ,²⁷ or to form $\text{Si}-\text{N}$ ^{28,29} or $\text{C}-\text{N}$ bonds.^{30–32} Additionally, a tantalum compound featuring a side-on, end-on coordination mode of the $\mu\text{-N}_2$ ligand participates in hydrosilylation and hydroborylation reactions, making either a $\text{Si}-\text{N}$ ^{33,34} or a $\text{B}-\text{N}$ ^{35,36} bond while cleaving the $\text{N}-\text{N}$ bond.

One potential though rarely investigated method to initiate reactions of $\mu\text{-N}_2$ complexes is photochemical activation of the $\text{N}-\text{N}$ bond.³⁷ To our knowledge only one experimentalist has adopted this strategy; Floriani reported an example of photochemical $\text{N}-\text{N}$ bond cleavage involving the thermally stable compound $(\mu\text{-N}_2)[\text{Mo}(\text{Mes})_3]_2$ ($\text{Mes} = 2,4,6\text{-Me}_3\text{C}_6\text{H}_2$).³⁸ Photolysis of this compound yields 1 equiv of $(\mu\text{-N})[\text{Mo}(\text{Mes})_3]_2$ while liberating 0.5 equiv of N_2 . Although the photochemistry of transition metal $\mu\text{-N}_2$ complexes is sparsely explored,

productive photochemistry of N_2 has been developed. For example, under photochemical conditions, either TiO_2 doped with Fe_2O_3 ^{39–41} or C_{60} encapsulated in two γ -cyclodextrin molecules⁴² are reported to catalyze the conversion of N_2 to NH_3 .

Three-coordinate molybdenum trisilanide, $\text{Mo}(\text{N}[\text{t-Bu}]\text{Ar})_3$, **1**, has been important in defining thermal $6e$ reduction chemistry of N_2 by cleavage of the $\text{N}-\text{N}$ triple bond.^{7,10,11,17} Dinitrogen is bound by 2 equiv of $\text{Mo}(\text{N}[\text{t-Bu}]\text{Ar})_3$ to form the thermally unstable intermediate, $(\mu\text{-N}_2)[\text{Mo}(\text{N}[\text{t-Bu}]\text{Ar})_3]_2$, **2**, which undergoes homolytic fragmentation of the $\text{N}-\text{N}$ bond to form 2 equiv of $\text{N}\equiv\text{Mo}(\text{N}[\text{t-Bu}]\text{Ar})_3$, **3** (Scheme 1). Although several well-defined metal reagents will cleave the $\text{N}-\text{N}$ bond of N_2 to produce either terminal or bridging nitride products,^{10,11,38,43–47} the case for **1** remains exceptional in that the metal fragment that binds N_2 , **1**, and the dinitrogen complex intermediate, **2**, en route to nitride formation can be isolated and studied. These criteria make **2** an ideal candidate for investigating homolytic fragmentation of the $\text{N}-\text{N}$ bond uncomplicated by other processes. As a result, this reaction sequence has been the topic of numerous mechanistic^{10,16,48} and theoretical investigations.^{49–56}

- (20) Smith, J. M.; Sadique, A. R.; Cundari, T. R.; Rodgers, K. R.; Lukat-Rodgers, G.; Lachicotte, R. J.; Flaschenriem, C. J.; Vela, J.; Holland, P. L. *J. Am. Chem. Soc.* **2006**, *128*, 756–769.
- (21) Chomitz, W. A.; Arnold, J. *Chem. Commun.* **2007**, 4797–4799.
- (22) Kilgore, U. J.; Yang, X.; Tomaszewski, J.; Huffman, J. C.; Mindiola, D. J. *Inorg. Chem.* **2006**, *45*, 10712–10721.
- (23) Jolly, P. W.; Jonas, K.; Krüger, C.; Tsay, Y.-H. *J. Organomet. Chem.* **1971**, *33*, 109–122.
- (24) Betley, T. A.; Peters, J. C. *J. Am. Chem. Soc.* **2004**, *126*, 6252–6254.
- (25) Vidyaratne, I.; Gambarotta, S.; Korobkov, I.; Budzelaar, P. H. M. *Inorg. Chem.* **2005**, *44*, 1187–1189.
- (26) MacLachlan, E. A.; Fryzuk, M. D. *Organometallics* **2006**, *25*, 1530–1543.
- (27) Pool, J. A.; Lobkovsky, E.; Chirik, P. J. *Nature* **2004**, *427*, 527–530.
- (28) Basch, H.; Musaev, D. G.; Morokuma, K.; Fryzuk, M. D.; Love, J. B.; Seidel, W. W.; Albinati, A.; Koetzle, T. F.; Klooster, W. T.; Mason, S. A.; Eckert, J. *J. Am. Chem. Soc.* **1999**, *121*, 523–528.
- (29) Fryzuk, M. D.; Love, J. B.; Rettig, S. J.; Young, V. G. *Science* **1997**, *275*, 1445–1447.
- (30) Bernskoetter, W. H.; Lobkovsky, E.; Chirik, P. J. *Angew. Chem., Int. Ed.* **2007**, *46*, 2858–2861.
- (31) Morello, L.; Love, J. B.; Patrick, B. O.; Fryzuk, M. D. *J. Am. Chem. Soc.* **2004**, *126*, 9480–9481.
- (32) Bernskoetter, W. H.; Olmos, A. V.; Pool, J. A.; Lobkovsky, E.; Chirik, P. J. *J. Am. Chem. Soc.* **2006**, *128*, 10696–10697.
- (33) Fryzuk, M. D.; MacKay, B. A.; Patrick, B. O. *J. Am. Chem. Soc.* **2003**, *125*, 3234–3235.
- (34) MacKay, B. A.; Munha, R. F.; Fryzuk, M. D. *J. Am. Chem. Soc.* **2006**, *128*, 9472–9483.
- (35) Fryzuk, M. D.; MacKay, B. A.; Johnson, S. A.; Patrick, B. O. *Angew. Chem., Int. Ed.* **2002**, *41*, 3709–3712.
- (36) MacKay, B. A.; Johnson, S. A.; Patrick, B. O.; Fryzuk, M. D. *Can. J. Chem.* **2005**, *83*, 315–323.
- (37) Reiher, M.; Kirchner, B.; Dieter, J. H.; Bernd, S.; Hess, A. *Chem.—Eur. J.* **2004**, *10*, 4443–4453.
- (38) Solari, E.; Da Silva, C.; Iacono, B.; Hesschenbrouck, J.; Rizzoli, C.; Scopelliti, R.; Floriani, C. *Angew. Chem., Int. Ed.* **2001**, *40*, 3907–3909.

- (39) Schrauzer, G. N.; Guth, T. D. *J. Am. Chem. Soc.* **1977**, *99*, 7189–7193.
- (40) Rusina, O.; Eremenko, A.; Frank, G.; Strunk, H. P.; Kisch, H. *Angew. Chem., Int. Ed.* **2001**, *40*, 3993–3995.
- (41) Rusina, O.; Linnik, O.; Eremenko, A.; Kisch, H. *Chem.—Eur. J.* **2003**, *9*, 561–565.
- (42) Nishibayashi, Y.; Saito, M.; Uemura, S.; Takekuma, S.; Takekuma, H.; Yoshida, Z. *Nature* **2004**, *428*, 279–280.
- (43) Clentsmith, G. K. B.; Bates, V. M. E.; Hitchcock, P. B.; Cloke, F. G. N. *J. Am. Chem. Soc.* **1999**, *121*, 10444–10445.
- (44) Kawaguchi, H.; Matsuo, T. *Angew. Chem., Int. Ed.* **2002**, *41*, 2792–2794.
- (45) Fryzuk, M. D.; Kozak, C. M.; Bowdridge, M. R.; Patrick, B. O.; Rettig, S. J. *J. Am. Chem. Soc.* **2002**, *124*, 8389–8397.
- (46) Berno, P.; Gambarotta, S. *Organometallics* **1995**, *14*, 2159–2161.
- (47) Vidyaratne, I.; Crewdson, P.; Lefebvre, E.; Gambarotta, S. *Inorg. Chem.* **2007**, *46*, 8836–8842.
- (48) Tsai, Y.-C.; Cummins, C. C. *Inorg. Chim. Acta* **2003**, *345*, 63–69.
- (49) Cui, Q.; Musaev, D. G.; Svensson, M.; Sieber, S.; Morokuma, K. *J. Am. Chem. Soc.* **1995**, *117*, 12366–12367.
- (50) Christian, G.; Stranger, R.; Yates, B. F.; Graham, D. C. *Dalton Trans.* **2005**, 962–968.
- (51) Christian, G.; Driver, J.; Stranger, R. *Faraday Discuss.* **2003**, *124*, 331–341.
- (52) Graham, D. C.; Beran, G. J. O.; Head-Gordon, M.; Christian, G.; Stranger, R.; Yates, B. F. *J. Phys. Chem. A* **2005**, *109*, 6762–6772.
- (53) Christian, G.; Stranger, R. *Dalton Trans.* **2004**, 2492–2495.
- (54) Neyman, K. M.; Nasluzov, V. A.; Hahn, J.; Landis, C. R.; Rosch, N. *Organometallics* **1997**, *16*, 995–1000.
- (55) Hahn, J.; Landis, C. R.; Nasluzov, V. A.; Neyman, K. M.; Rosch, N. *Inorg. Chem.* **1997**, *36*, 3947–3951.
- (56) Marcus, C. D. *Chem.—Eur. J.* **2007**, *13*, 3406–3413.

In particular, the molecular structure and dynamics of **2** have been the subject of much speculation.^{49–56}

In this work, two X-ray crystal structures of **2** have been solved to address detailed structural aspects of this key intermediate in thermal N₂ cleavage. A new protocol was developed for isolating **2** as a pure material, and with **2** in hand its reaction chemistry has been studied. Oxidation of **2** by either 1e or 2e affords isolable products, both of which have been structurally characterized. Comparison between these oxidation products and **2** offers insight into bonding within the MoNNMo core. Furthermore, a photochemical reaction of **2** is reported in which competition between N–N bond cleavage and N₂ extrusion forms both **1** and **3**.

Results and Discussion

Structure and Magnetism of 2. We have shown in a prior EXAFS (extended X-ray absorption fine structure) study that **2** adopts a conformation wherein the six *tert*-butyl groups are directed inward, toward a linear MoNNMo core of the molecule, and the six aryl rings are directed away from the center of the molecule. A number of computational studies have interrogated our structural model for **2** as well as those conformers that arise from rotation of one or more anilide ligands about the Mo–N bonds. One such investigation showed that rotation of a single anilide ligand by 180° away from the structure described is energetically uphill.⁵⁵ By further exploring the effects of anilide-ligand rotation, a recent theoretical study predicted a stable minimum for a *diamagnetic* conformer in which two opposing anilide ligands are rotated by 90°. ^{50–53} Moreover, such a quasi-C_{2h} structure was predicted to be lower in energy than the trigonal arrangement in which all *tert*-butyl groups are directed inward toward the center of the molecule. In addition to a 90° rotation of two anilide ligands, this conformation was found to possess a trans-bent MoNNMo core. The calculated bond angles around the μ-N₂ ligand (Mo–N–N) were 175° or 164° for **2** and a model complex, respectively. Interestingly, such a geometry deviates from the linear MoNNMo core that is found for related, structurally characterized μ-N₂ compounds of molybdenum,^{38,57,58} but recalls the zig-zag transition state structure for the N₂ cleavage reaction shown in Scheme 1.^{10,49}

To obtain more detailed structural data for **2** than in the prior EXAFS study, single crystals of **2** were grown for the purpose of X-ray diffraction. When solutions of **1** in a mixture of MesCN/MeCy/O(SiMe₃)₂ were stored under an atmosphere of N₂ at –35 °C, we obtained purple crystals of **2** suitable for X-ray diffraction. In the crystal structure, 2 equiv of O(SiMe₃)₂ pack with each equiv of **2** (Figure 1). The six anilide ligands are arranged with the *tert*-butyl groups directed toward the center of the molecule that features a linear MoNNMo core: Mo–N–N, 179.87(14)°. Three anilide ligands are arranged in a trigonal conformation around each Mo center, with the three aryl substituents forming a C₃ propeller. The crystallographic C₂ axis, that is orthogonal to the N–N vector, requires the two C₃ propellers to turn with the same chirality. The metrical parameters obtained via single crystal X-ray diffraction (Table 1) are in close agreement with previously obtained EXAFS data for frozen solutions of **2**. The EXAFS data indicated a linear MoNNMo core defined by a Mo–Mo separation of 4.94 Å and N–N internuclear distance of 1.19(2) Å.¹⁰

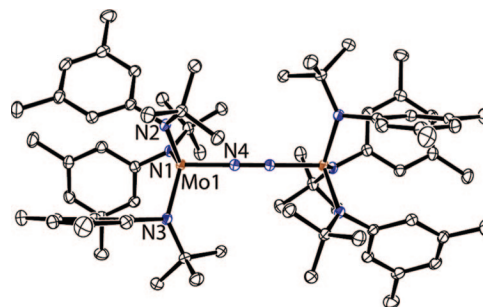


Figure 1. The molecular structure of **2** is shown with thermal displacement ellipsoids at the 50% probability level. Hydrogen atoms have been omitted for clarity. Crystal parameters are *P2*/*n*: *a* = 19.3 Å, *b* = 11.5 Å, *c* = 21.1 Å, β = 99.2°, and a crystallographically imposed two-fold axis relates the two halves of the molecule. A chemically equivalent but crystallographically distinct structure is described in detail in the Supporting Information.

Table 1. Comparison of Internuclear Distances (Å) for [(μ-N₂)[Mo(N[*t*-Bu]Ar)₃]₂]^{*n*+} (*n* = 0, 1, 2)

compound	2	2	2[B(Ar ^F) ₄]	2[B(Ar ^F) ₄] ₂
space group	<i>P2</i> / <i>n</i>	<i>P2</i> / <i>n</i>	<i>P2</i> / <i>1</i> / <i>n</i>	<i>P2</i> / <i>1</i> / <i>n</i>
N–N	1.212(2)	1.217(2)	1.239(4)	1.265(5)
Mo–N	1.868(1)	1.870(2)	1.835(3)	1.798(2)
		1.872(2)	1.841(3)	
Mo–Mo	4.9476(5)	4.958(2)	4.9151(6)	4.8599(5)
Mo–N[<i>t</i> -Bu]Ar (avg)	1.985(2)	1.986(2)	1.956(3)	1.931(3)

We found that **2** could also be crystallized from solutions of **1** in *n*-pentane/O(SiMe₃)₂ when stored under N₂ at –35 °C. The X-ray structure obtained using crystals so obtained indicated that *n*-pentane was incorporated into the crystal packing. This second molecular structure of **2** has a pseudo-C₂ axis, although no crystallographically imposed symmetry element bisects the molecule; each atom is crystallographically independent. Comparison between the two X-ray crystal structures reveals no significant differences in the molecular structure of **2** (Table 1).

Computational studies predicted that **2** exists as a triplet (*S* = 1) at 20 °C when the anilide ligands adopt the observed, trigonal arrangement.^{49–51,54,55} These predictions agree with the previous experimental observation that (μ-N₂)[Mo(N[*t*-Bu]Ph)₃]₂ exists as a triplet (*S* = 1) at 20 °C.¹⁰ However, the proposal that **2** and (μ-N₂)[Mo(N[*t*-Bu]Ph)₃]₂ should exhibit similar magnetic properties was recently challenged.⁵⁰ It was predicted that the bulky Ar groups of **2** force a pair of inversion-related anilide ligands to rotate such that their NC₂ planes become orthogonal to the MoNNMo axis, and that this ligand rotation coincides with a change in the magnetic ground state. The resulting change in the calculated singlet–triplet gap was dramatic: 1922 cm^{–1} for **2** compared to 585 cm^{–1} for (μ-N₂)[Mo(N[*t*-Bu]Ph)₃]₂.⁵⁰ To test this intriguing prediction, magnetic studies now have been carried out on **2**.

To address experimentally the magnetism of **2**, the variable-temperature bulk magnetism of **2** was measured by SQUID magnetometry.⁵⁹ A plot of μ_{eff} vs *T* plateaus at a maximum value of μ_{eff} = 2.40 μ_B (Figure 2). This value is lower than the expected spin-only value of 2.83 μ_B corresponding to a triplet

(57) Greco, G. E.; Schrock, R. R. *Inorg. Chem.* **2001**, *40*, 3861–3878.

(58) Shih, K.-Y.; Schrock, R. R.; Kempe, R. *J. Am. Chem. Soc.* **1994**, *116*, 8804–8805.

(59) O'Connor, C. J. In *Molecule-Based Magnetic Materials*; Turnbull, M. M., Sugimoto, T., Thompson, L. K., Eds.; American Chemical Society: Washington, DC, 1996; p 44–66.

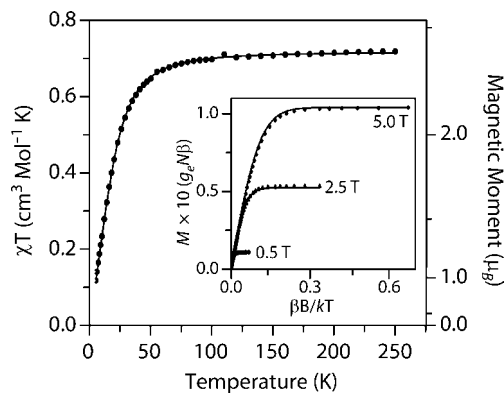


Figure 2. Dependence of the magnetic moment of **2** upon temperature as measured by SQUID magnetometry. The inset shows molar magnetization of **2** as a function of both temperature and field strength. The magnetic data were fit to a spin Hamiltonian for an $S = 1$ state with zero-field splitting. The parameters for the fits shown above are $g = 1.69$ and $D = 42 \text{ cm}^{-1}$. Contributions made by temperature-independent paramagnetism were fit and subtracted from the data. N is Avogadro's number, β is the Bohr magneton, and k is Boltzmann's constant.

($S = 1$) spin system.^{60–62} Moreover, the magnetic moment rapidly declines when the temperature is reduced below 50 K. To pinpoint the physical origin of the magnetic behavior at low temperatures, magnetic data were acquired on a single sample at three fields (0.5, 2.5, and 5.0 T) over a temperature range of 0–250 K. The plot of molar magnetization (M) vs $\beta B/kT$ reaches a different maximum value at each field strength (Figure 2, inset). This finding suggested that the decline of the magnetic moment at low temperatures is due to sizable zero-field splitting of a ground-state triplet.⁶³ Accordingly, the variable-temperature, variable-field data were fit to an $S = 1$ spin Hamiltonian to provide the zero-field splitting parameter, $D = 42 \text{ cm}^{-1}$, and the gyromagnetic ratio, $g = 1.69$ using the julX software package.⁶⁴ The positive sign of the zero-field splitting parameter, D , indicates that the $m_s = 0$ level of the triplet state lies lower in energy than the $m_s = -1, 1$ level. At low temperatures and low magnetic fields the $m_s = -1, 1$ levels are depopulated and the magnetization is correspondingly decreased. The g value of 1.69 is lower than the Landé g_e , reflecting the axial anisotropy that is suggested by the value of D .⁶⁵ Moreover, the value obtained for g predicts a maximum spin-only magnetic moment of $2.39 \mu_B$ (via $\mu_{\text{eff}} = g \times (S(S+1))^{1/2}$) which agrees well with the observed value near 300 K. Using an alternative model provided by the Bleaney–Bowers equation^{66,67} resulted in a less satisfactory fit of the magnetic data and fails to account for the field-dependence of the molar magnetization (Figure S19). Therefore, we conclude that **2** has an isolated triplet ($S =$

1) ground-state that is best described by a 42 cm^{-1} separation between the low lying $m_s = 0$ and degenerate $m_s = -1, 1$ levels in the absence of an applied field.

Mechanism of Thermal N–N Bond Cleavage. A zig-zag transition state structure, 2^\ddagger , has been proposed as part of a mechanism for the required transit between the triplet and singlet electronic surfaces that relate **2** and 2 equiv of **3** (Scheme 1).^{10,49,54,68,69} This transition-state model is a common feature among theoretical analyses of thermal N–N bond cleavage by **2**. Additionally, analogous zig-zag structures have been proposed for the dimerization of two terminal nitriles to form a $\mu\text{-N}_2$ complex.^{24,70–73} For these reasons, it is noteworthy that the singlet molecule, featuring a pair of inversion-related anilide ligands rotated such that their NC_2 planes become orthogonal to the MoNNMo axis as located by Stranger and co-workers, contains both this MoNNMo zig-zag structure and a longer N–N bond than the observed, linear geometry.^{50–53} Although this computationally predicted conformation for **2** agrees with neither the structural nor magnetic data obtained from authentic samples of **2** we still found the structural relationship between the putative zig-zag transition state en route to cleavage of the N–N bond and this proposed geometry intriguing.^{50,51}

Rotation of one or more anilide ligands has previously not been considered as a structural feature of the zig-zag transition state, 2^\ddagger . Via ligand rotation, one of the metal π -symmetry (with respect to the $\mu\text{-N}_2$ ligand) orbitals is destabilized and the orbital degeneracies that exist in pseudo- C_3 coordination geometries are lifted. If one could show that ligand rotation were coupled to the formation of a zig-zag structure of 2^\ddagger then this would be of mechanistic interest with regard to N_2 cleavage. In this regard, one expects the barrier to ligand rotation in **2** to be greater in energy than for less sterically crowded ($\mu\text{-N}_2$)[Mo(N[*i*-Pr]Ar)₃]₂. Interestingly, ($\mu\text{-N}_2$)[Mo(N[*i*-Pr]Ar)₃]₂ has never been directly observed as an intermediate in the N_2 -cleavage reaction carried out by HMo($\eta^2\text{-Me}_2\text{CNAr}$)(N[*i*-Pr]Ar)₂.^{74,75} The accordingly inferred instability of ($\mu\text{-N}_2$)[Mo(N[*i*-Pr]Ar)₃]₂ is in sharp contrast with the properties of **2**, which can be isolated and studied as a pure material. We have suggested that facile N_2 cleavage by ($\mu\text{-N}_2$)[Mo(N[*i*-Pr]Ar)₃]₂ indicates that this compound more readily accommodates geometric changes along the reaction coordinate than does **2**.^{76,77}

The structure of ($\mu\text{-N}_2$)[Mo(R)(N(CH₂)₂)₃N]₂ (R = Me₂*t*-Bu)Si) has been compared with the structure of **2** previously.¹⁰ The two compounds have magnetic moments consistent with an $S = 1$ state and similar structural parameters. However, ($\mu\text{-N}_2$)[Mo(R)(N(CH₂)₂)₃N]₂ does not undergo thermal fragmentation with N–N bond cleavage.⁵⁸ We suggest that the chelating

- (60) O'Connor, C. J. In *Prog. Inorg. Chem.*; Lippard, S. J., Ed.; John Wiley & Sons, Inc.: New York, 1982; Vol. 29, p 203–283.
- (61) Van Vleck, J. H. *The Theory of Electric and Magnetic Susceptibilities*; Oxford University Press: New York, 1965; p 282–297.
- (62) Ballhausen, C. J. *Introduction to Ligand Field Theory*; McGraw-Hill: New York, 1962; p 139–151.
- (63) Girerd, J.-J.; Journaux, Y. In *Physical Methods in Bioinorganic Chemistry*; Lawrence Que, J., Ed.; University Science Books: Sausalito, CA, 2000; p 336–342.
- (64) Bill, E. *JulX 1.4, A Program for the Simulation and Analysis of Magnetic Susceptibility Data*; Max Plank Institute for Bioinorganic Chemistry: Mülheim an der Ruhr, 2008 (http://ewww.mpi-muelheim.mpg.de/bac/logins/bill/julX_en.php).
- (65) Kahn, O. *Molecular Magnetism*; VCH Publishers: New York, 1993.
- (66) Bleaney, B.; Bowers, K. D. *Proc. R. Soc. London, Ser. A* **1952**, *214*, 451–461.
- (67) Kahn, O. *Molecular Magnetism*; VCH Publishers: New York, 1993; p 103–134.

- (68) Woodward, R. B.; Hoffmann, R. *Angew. Chem., Int. Ed.* **1969**, *8*, 781–853.
- (69) Veige, A. S.; Slaughter, L. M.; Lobkovsky, E. B.; Wolczanski, P. T.; Matsunaga, N.; Decker, S. A.; Cundari, T. R. *Inorg. Chem.* **2003**, *42*, 6204–6224.
- (70) Ware, D. C.; Taube, H. *Inorg. Chem.* **1991**, *30*, 4605–4610.
- (71) Seymore, S. B.; Brown, S. N. *Inorg. Chem.* **2002**, *41*, 462–469.
- (72) Seymore, S. B.; Brown, S. N. *Inorg. Chem.* **2006**, *45*, 9540–9550.
- (73) Man, W. L.; Tang, T. M.; Wong, T. W.; Lau, T. C.; Peng, S. M.; Wong, W. T. *J. Am. Chem. Soc.* **2004**, *126*, 478–479.
- (74) Tsai, Y.-C.; Johnson, M. J. A.; Mindiola, D. J.; Cummins, C. C.; Klooster, W. T.; Koetzle, T. F. *J. Am. Chem. Soc.* **1999**, *121*, 10426–10427.
- (75) Cherry, J.-P. F.; Stephens, F. H.; Johnson, M. J. A.; Diaconescu, P. L.; Cummins, C. C. *Inorg. Chem.* **2001**, *40*, 6860–6882.
- (76) Hammond, G. S. *J. Am. Chem. Soc.* **1955**, *77*, 334–338.
- (77) Carey, F. A.; Sundberg, R. J. *Advanced Organic Chemistry Part A: Structure and Mechanism*; Kluwer Academic/Plenum Publishers: New York, 2000; p 217–222.

arms of the [(R)N(CH₂)₂]₃N ligand inhibit rotation about the Mo–N_{amm} bond. If ligand rotation is important for accommodating transit between the triplet and singlet spin-states, then fundamental differences in the reaction chemistry of these two closely related molecules might be explained in terms of ancillary ligand structural constraints. Alternatively, this difference might also be the result of the apical-nitrogen donor that is present in (μ-N₂)[Mo[(R)N(CH₂)₂]₃N]₂ but absent in **2**.⁴⁹

Solid-State Stability of 2 and Structure of Crystalline 3. In solution, **2** readily fragments to yield 2 equiv of **3** (*t*_{1/2} ≈ 30 min, 25 °C).¹⁰ Having obtained for the first time samples of **2** as single crystals, we became curious as to whether the extended crystal lattice would confer additional stability to **2**.^{78–83} Crystals of **2** (ca. 0.25 × 0.20 × 0.20 mm³), grown from *n*-pentane/O(SiMe₃)₂, were stored at 20 °C under light petroleum oil for 24 h. After that time, the crystals continued to diffract and the unit cell was measured. The measured unit cell parameters in *P*2₁/*n* were unchanged in comparison to those found for fresh crystals that had been analyzed 24 h earlier. These crystals were additionally suspended in nujol oil and monitored by UV–vis spectroscopy at 20 °C over 22 h. During that time no change had occurred in the absorbance spectrum. These two observations suggest that in comparison to solutions or amorphous solids, the extended structure of the crystal lattice stabilizes **2** with respect to fragmentation.⁸⁴

The terminal nitride, **3**, formed by thermal fragmentation of **2**, has not been structurally characterized in the past due to a severe crystallographic disorder. Here we report the first satisfactory solution to X-ray diffraction data. Crystals of **3** were grown from *n*-pentane/Et₂O at –35 °C. It was found that slow cooling of a pale yellow crystal of **3** from 20 to –173 °C was essential to prevent cracking of the crystal, allowing X-ray diffraction data to be collected. A satisfactory solution to the X-ray diffraction data was found in the space group *P*2₁/*n*. This solution contains four crystallographically independent molecules per asymmetric unit, two of which are highly disordered. Each molecule of **3** approximates C₃ symmetry in the solid state, as the aryl rings are staggered in the same direction (Figure 3). The analogous compound, N≡Mo(N[*t*-Bu]Ph)₃, is not subject to the same crystallographic disorder, and its X-ray crystal structure has been previously reported.¹⁰ Therefore, the metrical parameters of this compound may be compared to those of **3**. For **3**, the Mo≡N bond length is 1.651(4) Å while the average Mo–N[*t*-Bu]Ar bond length is 1.964(4) Å. These values are closely approximated by those found for N≡Mo(N[*t*-Bu]Ph)₃ for which the Mo≡N internuclear distance is 1.658(5) Å and one Mo–N[*t*-Bu]Ph distance is 1.979(2) Å.¹⁰

Redox Chemistry of (μ-N₂)[Mo(N[*t*-Bu]Ar)₃]₂. We envisioned that by removing 2e from **2**, the corresponding formal *d*²–*d*² compound should be thermally stable because too few electrons are present to engage in 6e reductive cleavage of the N–N bond. Moreover, a thermally stable, dicationic compound might be useful for the storage and in situ generation of **2**. With isolated **2** in hand, the 2e oxidation was carried out by addition of **2** to a solution containing 2 equiv of [Cp₂Fe][B(Ar^F)₄] (Cp = η⁵-

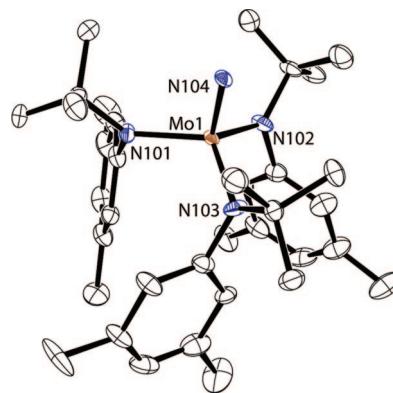
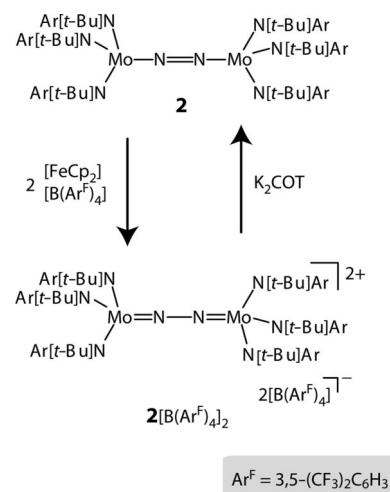


Figure 3. The molecular structure of **3** is shown with thermal displacement ellipsoids at the 50% probability level. Hydrogen atoms have been omitted for clarity.

Scheme 2



C₅H₅, Ar^F = 3,5-C₆H₃(CF₃)₂). When the oxidation is carried out in Et₂O, (μ-N₂)[Mo(N[*t*-Bu]Ar)₃]₂[B(Ar^F)₄]₂, **2**[B(Ar^F)₄]₂, is collected by filtration as a red powder in 98% yield (Scheme 2). Powders or CH₂Cl₂ solutions of **2**[B(Ar^F)₄]₂ may be stored at 20 °C for greater than 5 d without significant decomposition.

Reduction of **2**[B(Ar^F)₄]₂ to return **2** was effected by the soluble reducing agent K₂COT (COT = C₈H₈).⁸⁵ This reducing agent was desirable because it is soluble in THF^{86,87} and has a sufficient reduction potential to carry out both reduction steps to form **2** while avoiding reduction of **2** to form 2 equiv of [K][NNMo(N[*t*-Bu]Ar)₃].^{88–91} Reduction of **2**[B(Ar^F)₄]₂ by K₂COT proceeds rapidly in THF solutions to form **2** as the only molybdenum-containing product (Scheme 2). Using this procedure, **2** may be obtained in 85% isolated yield, after separation from the K[B(Ar^F)₄] and COT byproducts.

(85) Katz, T. J. *J. Am. Chem. Soc.* **1960**, *82*, 3784–3785.

(86) Stevenson, G. R.; Ocasio, I. *J. Phys. Chem.* **1975**, *79*, 1387–1390.

(87) Cox, R. H.; Harrison, L. W.; Austin, W. K. *J. Phys. Chem.* **1973**, *77*, 200–204.

(88) Allendoerfer, R. D. *J. Am. Chem. Soc.* **1975**, *97*, 218–219.

(89) Allendoerfer, R. D.; Rieger, P. H. *J. Am. Chem. Soc.* **1965**, *87*, 2336–2344.

(90) Katz, T. J.; Reinmuth, W. H.; Smith, D. E. *J. Am. Chem. Soc.* **1962**, *84*, 802–808.

(91) We measured an *E*_{1/2} of –2.9 V (vs Cp₂Fe⁺⁰/O) for the first 1e oxidation of K₂COT in 0.2 M [(*n*-Bu)₄N][PF₆]/THF.

(78) Ramamurthy, V.; Venkatesan, K. *Chem. Rev.* **1987**, *87*, 433–481.

(79) Buergi, H. B.; Dunitz, J. D. *Acc. Chem. Res.* **1983**, *16*, 153–161.

(80) Ohashi, Y. *Acc. Chem. Res.* **1988**, *21*, 268–274.

(81) Ohashi, Y.; Sasada, Y. *Nature* **1977**, *267*, 142–144.

(82) Ohashi, Y.; Yanagi, K.; Kurihara, T.; Sasada, Y.; Ohgo, Y. *J. Am. Chem. Soc.* **1981**, *103*, 5805–5812.

(83) Paul, I. C.; Curtin, D. Y. *Acc. Chem. Res.* **1973**, *6*, 217–225.

(84) Ozerov, O. V.; Guo, C.; Papkov, V. A.; Foxman, B. M. *J. Am. Chem. Soc.* **2004**, *126*, 4792–4793.

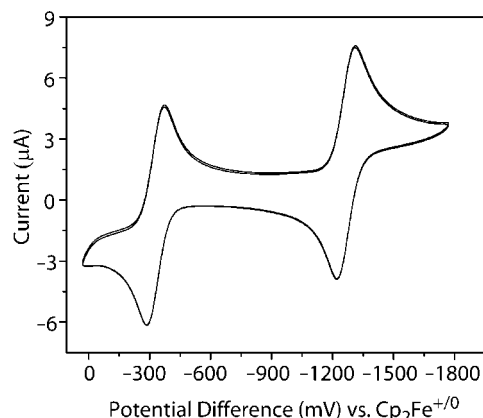
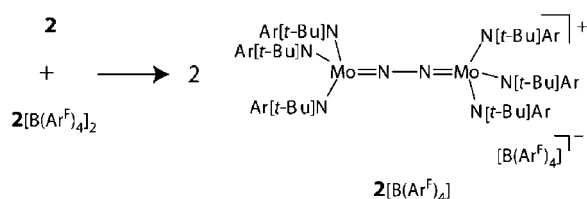


Figure 4. The cyclic voltammogram of $2[\text{B}(\text{Ar}^{\text{F}})_4]_2$ in 0.1 M $[(\text{N}(\text{n-Bu})_4)[\text{B}(\text{C}_6\text{F}_5)_4]/\text{THF}]^{92,93}$ shows two reversible redox events. Assignment of each event is given in the text.

Scheme 3



Two reversible 1e processes are observed in the cyclic voltammogram of $2[\text{B}(\text{Ar}^{\text{F}})_4]_2$ (Figure 4).^{92,93} These are assigned to the $2^{2+}/2^+$ couple at -320 mV and $2^+/2$ couple at -1460 mV, where $\text{Cp}_2\text{Fe}^{+/0} = 0$ mV. The $2^+/2$ couple has previously been observed in the cyclic voltammogram of 2 .¹⁶ From a qualitative point of view, 2 is about as reducing as Cp_2Co .⁹⁴

The separation between the two reversible 1e processes observed in the cyclic voltammogram is related to the ΔG° for the comproportionation between 2 and 2^{2+} to form 2 equiv of 2^+ .^{95–97} From the peak separation of 1.14 V, the equilibrium constant for this reaction was calculated to be $K_{\text{eq}} = 1.9 \times 10^{19}$.^{96–99} Comproportionation served as a viable synthetic route to $(\mu\text{-N}_2)[\text{Mo}(\text{N}[\text{t-Bu}]\text{Ar})_3]_2[\text{B}(\text{Ar}^{\text{F}})_4]_2$, $2[\text{B}(\text{Ar}^{\text{F}})_4]$: Addition of $2[\text{B}(\text{Ar}^{\text{F}})_4]_2$ to a solution of 2 rapidly formed the mixed-valent compound, $2[\text{B}(\text{Ar}^{\text{F}})_4]$ which was isolated as a cranberry-red solid in 95% yield (Scheme 3). Proton NMR spectra of $2[\text{B}(\text{Ar}^{\text{F}})_4]$ show a broad *tert*-butyl resonance centered at 6.0 ppm. Addition of either 2 or $2[\text{B}(\text{Ar}^{\text{F}})_4]_2$ to solutions of $2[\text{B}(\text{Ar}^{\text{F}})_4]$ broadens the resonances observed by ^1H NMR spectroscopy, as is expected for degenerate electron transfer.^{100–102}

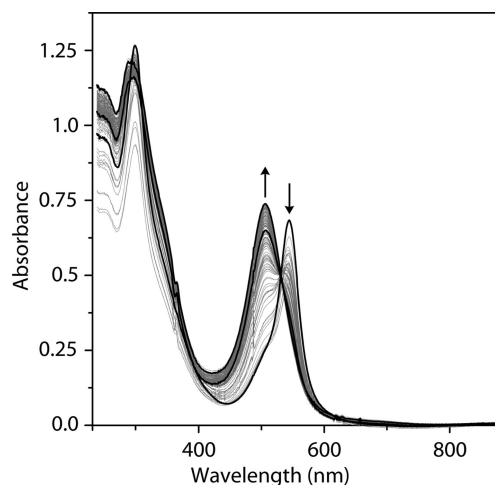


Figure 5. A spectroelectrochemical stack plot shows the conversion $2 \rightarrow 2^{2+}$ in 0.5 M $[\text{N}(\text{n-Bu})_4][\text{PF}_6]/\text{THF}$ in 0.5-s intervals.

We discovered that 2^+ is formed when 2 is dissolved in CDCl_3 as this solution quickly changes in color from purple to cranberry-red. Proton NMR, UV–vis, and Raman spectroscopy data support this conclusion, however the identity of the counteranion has not been investigated.

For $2[\text{B}(\text{Ar}^{\text{F}})_4]$, the magnetic moment of $1.96 \mu_{\text{B}}$ is consistent with one unpaired electron. This value, which is higher than the expected spin-only value of $1.73 \mu_{\text{B}}$, may indicate an orbital contribution from a 2E ground state (approximate C_3 symmetry is assumed) to the observed magnetic moment;^{103–105} however, care should be taken when interpreting these magnetic data because the measurement requires a large diamagnetic correction, $\chi_{\text{dia}} = -1.29 \times 10^{-3} \text{ cm}^3 \text{ Mol}^{-1}$ ($\chi_{\text{M}} = \chi_{\text{obs}} - \chi_{\text{dia}}$).⁶⁰

To further investigate the redox couples interrelating 2 , 2^+ , and 2^{2+} , the 2e oxidation of 2 was monitored spectroelectrochemically, allowing the visible transition of each chromophore to be compared in the same solvent and under the same experimental conditions.^{96,106} The oxidation of 2 in 0.5 M $[(\text{n-Bu})_4\text{N}][\text{PF}_6]/\text{THF}$ was monitored by UV–vis spectroscopy, while holding the spectroscopic cell at a potential of -200 mV. A stack plot of the UV–vis spectra, taken in 0.5-s intervals, shows the decay of 2 , which absorbs at 544 nm, accompanied by the growth of 2^+ absorbing at 506 nm (Figure 5). Changes in the absorbance are less dramatic as 2^+ is oxidized to form 2^{2+} because both species absorb strongly at 506 nm; however, the spectral features near 300 nm differ between the two. The spectral assignment for 2^+ was confirmed by measuring the UV–vis spectrum of 2^+ that was electrochemically generated from 2^{2+} in an optically transparent thin-layer electrochemical cell (see Supporting Information).^{107,108}

Solid State Structure of $2[\text{B}(\text{Ar}^{\text{F}})_4]$. Crystals of $2[\text{B}(\text{Ar}^{\text{F}})_4]$ for X-ray analysis were grown by vapor diffusion of *n*-pentane

- (92) LeSuer, R. J.; Buttolph, C.; Geiger, W. E. *Anal. Chem.* **2004**, *76*, 6395–6401.
 (93) LeSuer, R. J.; Geiger, W. E. *Angew. Chem., Int. Ed.* **2000**, *39*, 248–250.
 (94) Connelly, N. G.; Geiger, W. E. *Chem. Rev.* **1996**, *96*, 877–910.
 (95) Demadis, K. D.; Hartshorn, C. M.; Meyer, T. J. *Chem. Rev.* **2001**, *101*, 2655–2686.
 (96) Faulkner, L. R.; Bard, A. J. *Electrochemical Methods: Fundamentals and Applications*; 2nd ed.; Wiley: Hoboken, NJ, 2001; p 680–694.
 (97) Savéant, J.-M. *Elements of Molecular and Biomolecular Electrochemistry: An Electrochemical Approach to Electron Transfer Chemistry*; John Wiley & Sons: Hoboken, NJ, 2007; p 62–75.
 (98) Richardson, D. E.; Taube, H. *Inorg. Chem.* **1981**, *20*, 1278–1285.
 (99) Barriere, F.; Geiger, W. E. *J. Am. Chem. Soc.* **2006**, *128*, 3980–3989.
 (100) Dietrich, M. W.; Wahl, A. C. *J. Chem. Phys.* **1963**, *38*, 1591–1596.
 (101) Yang, E. S.; Chan, M.-S.; Wahl, A. C. *J. Phys. Chem.* **1975**, *79*, 2049–2052.

- (102) Yang, E. S.; Chan, M.-S.; Wahl, A. C. *J. Phys. Chem.* **1980**, *84*, 3094–3099.
 (103) Gray, H. B.; Hendrickson, D. N.; Sohn, Y. S. *Inorg. Chem.* **1971**, *10*, 1559–1563.
 (104) Sohn, Y. S.; Hendrickson, D. N.; Gray, H. B. *J. Am. Chem. Soc.* **1970**, *92*, 3233–3234.
 (105) Kramer, J. A.; Hendrickson, D. N. *Inorg. Chem.* **1980**, *19*, 3330–3337.
 (106) Rosenthal, J.; Lockett, T. D.; Hodgkiss, J. M.; Nocera, D. G. *J. Am. Chem. Soc.* **2006**, *128*, 6546–6547.
 (107) Pilkington, M. B. G.; Coles, B. A.; Compton, R. G. *Anal. Chem.* **1989**, *61*, 1787–1789.
 (108) Heineman, W. R.; Norris, B. J.; Goelz, J. F. *Anal. Chem.* **1975**, *47*, 79–84.

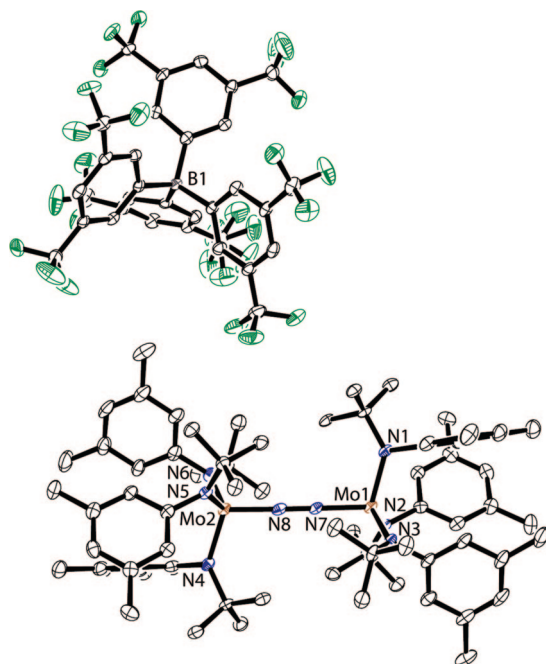


Figure 6. The molecular structure of $2[\text{B}(\text{Ar}^{\text{F}})_4]$ is shown with thermal displacement ellipsoids at the 50% probability level. Hydrogen atoms have been omitted for clarity.

into THF at 20 °C. All atoms are crystallographically independent in the space group $P2_1/n$, and the two Mo–N distances around the $\mu\text{-N}_2$ ligand, Mo(1)–N(7) and Mo(2)–N(8), are equivalent, within statistical error (Table 1, Figure 6). The MoNNMo core is nearly linear with Mo–N–N angles of 179.8(3)° and 178.7(3)°. A distortion breaking the trigonal symmetry around the MoNNMo core might be either small or a dynamic effect that is not observed.^{109–111}

The symmetrical bonding about the MoNNMo core in $2[\text{B}(\text{Ar}^{\text{F}})_4]$ contrasts other mixed-valent $\mu\text{-N}_2$ complexes that exhibit asymmetrical bonding about the $\mu\text{-N}_2$ ligand.^{112,113} Such complexes typically have a strong absorbance in the IR spectrum, whereas for $2[\text{B}(\text{Ar}^{\text{F}})_4]$ the N–N stretching mode is only Raman active (vide infra).¹¹² The symmetric bonding about the $\mu\text{-N}_2$ ligand in $2[\text{B}(\text{Ar}^{\text{F}})_4]$ is comparable with $[(\mu\text{-N}_2)(\text{M}(\text{NH}_3)_5)_2]^{5+}$ (M = Ru, Os), which have Raman active but IR inactive bands corresponding to the N–N normal mode. Therefore, structural characterization of $2[\text{B}(\text{Ar}^{\text{F}})_4]$ is consistent with a Robin–Day class III system in which the unpaired electron resides in a molecular orbital that is delocalized across the N–N bridge and is symmetrically shared by both metals.^{95,114} Absorbance bands in the near-IR region (700–3000 nm) were not located for $2[\text{B}(\text{Ar}^{\text{F}})_4]$. The lack of intense near-IR bands is consistent with the classification of $2[\text{B}(\text{Ar}^{\text{F}})_4]$ as a class III mixed valent complex, for which these bands can become exceedingly weak, hence unobserved.⁹⁵

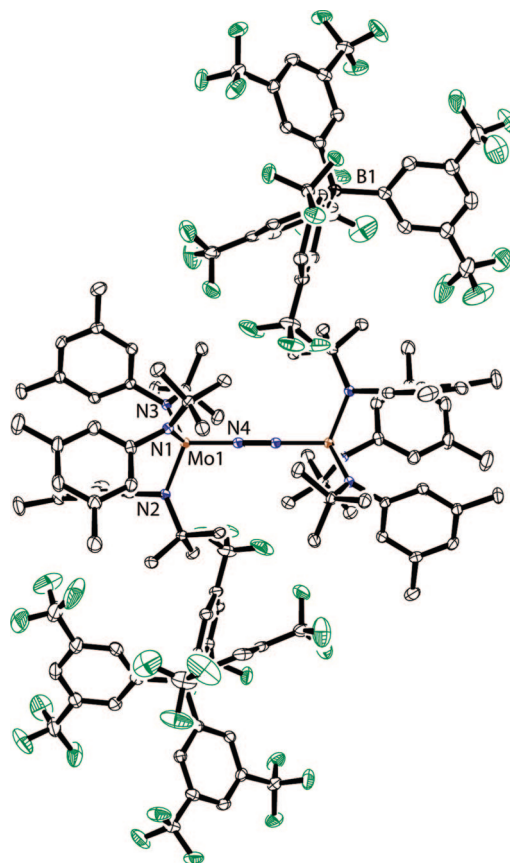


Figure 7. The molecular structure of $2[\text{B}(\text{Ar}^{\text{F}})_4]_2$ is shown with thermal displacement ellipsoids at the 50% probability level. Hydrogen atoms have been omitted for clarity.

Solid State Structure of $2[\text{B}(\text{Ar}^{\text{F}})_4]_2$. Crystals of $2[\text{B}(\text{Ar}^{\text{F}})_4]_2$, grown from THF/Et₂O/*n*-hexane at –35 °C, were suitable for X-ray diffraction. The molecular structure of $2[\text{B}(\text{Ar}^{\text{F}})_4]_2$ is symmetric about a crystallographic inversion center that is located on the N–N internuclear vector (Figure 7). The inversion center relates the two C_3 propellers formed by the staggered aryl rings, conferring a pseudo- S_6 geometry to the 2^{2+} ion. The short Mo–Mo distance of 4.86 Å suggests a congested ligand environment about the MoNNMo core (Table 1). Steric crowding is also evident in the ¹H NMR spectrum at 20 °C as two distinct resonances are observed for both the aromatic ortho- and aryl-methyl protons. These protons become magnetically inequivalent when the dynamic process that interconverts the two possible enantiomers defined by the C_3 aryl propellers is sufficiently hindered.

The N–N internuclear distance is a commonly used marker of N_2 activation when it is coordinated to a metal;^{2,115} therefore, it is worthwhile to compare the structures of $2[\text{B}(\text{Ar}^{\text{F}})_4]_2$, $2[\text{B}(\text{Ar}^{\text{F}})_4]$, and **2**. The N–N internuclear distance is longest in $2[\text{B}(\text{Ar}^{\text{F}})_4]_2$, 1.265(5) Å, while the N–N distance is ca. 0.026 Å shorter for $2[\text{B}(\text{Ar}^{\text{F}})_4]$ or ca. 0.051 Å shorter for **2**. The opposite trend is found for Mo–N internuclear distances; **2** has the longest Mo–N separation, 1.87 Å, when compared to the Mo–N distance in $2[\text{B}(\text{Ar}^{\text{F}})_4]$, 1.835(3) Å, or $2[\text{B}(\text{Ar}^{\text{F}})_4]_2$, 1.798(2) Å. Both trends indicate that the $\mu\text{-N}_2$ ligand becomes more activated by removing 2e from the π bonding MoNNMo core of **2**.¹¹⁵

(109) Jahn, H. A.; Teller, E. *Proc. R. Soc. London, A* **1937**, *161*, 220–235.

(110) Sugano, S.; Tanabe, Y.; Kamimura, H. *Multiplets of Transition-Metal Ions in Crystals*; Academic Press: New York, 1970, p 241–248.

(111) Bersuker, I. B. *Chem. Rev.* **2001**, *101*, 1067–1114.

(112) Demadis, K. D.; Meyer, T. J.; White, P. S. *Inorg. Chem.* **1997**, *36*, 5678–5679.

(113) Demadis, K. D.; El-Samanody, E. S.; Coia, G. M.; Meyer, T. J. *J. Am. Chem. Soc.* **1999**, *121*, 535–544.

(114) Robin, M. B.; Day, P. In *Adv. Inorg. Chem. Radiochem.*; Emeléus, H. J., Sharpe, A. G., Eds.; Academic Press: New York, 1967; Vol. 10, p 247–423.

(115) Fryzuk, M. D.; Johnson, S. A. *Coord. Chem. Rev.* **2000**, *200*, 379–409.

Activation of N_2 is generally achieved by reducing the N_2 , and it is noteworthy to recognize that a number of dicationic $\mu-N_2$ compounds are described in the literature. Schrock has reported the electrochemistry of $(\mu-N_2)[M((4-t-Bu)C_6H_4)NCH_2CH_2)_3N]_2$, $M = Mo, W$.⁵⁷ For the case of W , the neutral $\mu-N_2$ complex was cleanly oxidized by either 1e or 2e to afford isolable products; however, crystals suitable for X-ray diffraction studies could not be grown for these compounds. The compound $[(\mu-N_2)(W(dmpe)Cp^*)_2][B(C_6F_5)_4]_2$ ($Cp^* = \eta^5-(CCH_3)_5$, $dmpe = 1,2-(Me_2P)_2C_2H_4$), formed upon exposure of $[(\eta^7-C_5Me_3(CH_2)_2)(dmpe)W(H)_2][B(C_6F_5)_4]$ to N_2 , has an N–N separation of 1.22(1) Å and a W–N distance of 1.888(5) Å while the W–N–N angle is nearly linear, 176(7)°. ¹¹⁶ The dizwitterionic compound $(\mu-N_2)[Fe((i-Pr)_2PCH_2CH_2)_3BPh]_2$ shows significant activation of the N_2 ligand in its N–N distance of 1.138(6) Å and Fe–N separation of 1.815 Å (average of 2).²⁴ A recent EPR/Mössbauer study concluded that this compound is best described as an Fe(I)/Fe(II) ground-state septet.¹¹⁷ These examples demonstrate that marked reduction of the $\mu-N_2$ ligand may be present even when bound between two positively charged metal centers.

Raman Spectroscopy. Raman spectroscopy is a common marker of activation of the N_2 ligand,^{2,115} and Raman shifts are known to correlate well with N–N internuclear separation for a number of compounds containing the N_2 unit.^{10,118} The extent of activation of the N_2 ligand is typically measured against free N_2 which has a N–N separation of 1.0975 Å and Raman shift of 2331 cm^{-1} .^{119–121} To complement the trend in N–N internuclear distance for 2^{n+} ($n = 0, 1, 2$) as observed by X-ray crystallography (Table 1), Raman spectroscopy was carried out on these compounds.

Resonance Raman spectroscopy performed on $2[B(Ar^F)_4]_2$ ($\lambda_{excite} = 514.5$ nm) showed only one intense feature at 1349 cm^{-1} which was assigned to the Stokes shift for N–N polarization. This assignment was confirmed by the Raman shift for $[^{15}N-2][B(Ar^F)_4]_2$ which is found at 1305 cm^{-1} , 44 cm^{-1} less energetic than the shift observed for the lighter isotopomer. This decrease in the Raman shift upon isotopic labeling agrees with the change calculated for a harmonic oscillator.¹²² Raman spectroscopy of $2[B(Ar^F)_4]$ ($\lambda_{excite} = 785$ nm) showed an intense Stokes shift at 1503 cm^{-1} which was shifted to 1438 cm^{-1} for the ^{15}N isotopomer. The observed isotope shift of 65 cm^{-1} is greater than the calculated shift of 51 cm^{-1} , indicating a degree of anharmonic character in the vibration. Anharmonic potentials have been associated with a dynamic Jahn–Teller distortion.^{110,123}

The Raman spectrum of **2** contains the N–N bond polarization at 1630 cm^{-1} .¹⁰ The lower energy polarizations of 1503 and 1349 cm^{-1} for $2[B(Ar^F)_4]$ and $2[B(Ar^F)_4]_2$, respectively, are consistent with a weakening of the N–N bond upon oxidation of **2**.^{2,115} These Raman shifts may be plotted as a function of N–N internuclear distance (Figure 8),¹¹⁸ moreover

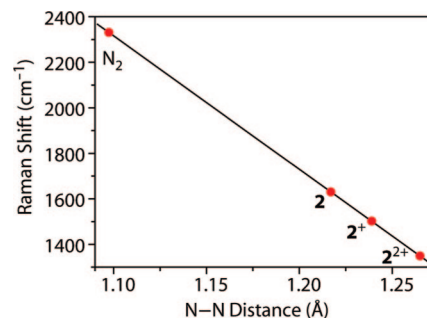


Figure 8. Raman shifts plotted as a function of N–N internuclear distance. The best fit line through four points is given by $\nu(r) = -5859r + 8762$, $R^2 = 1.000$, $\sigma = 1.04$ cm^{-1} . Raman shifts are given in the text and bond lengths are listed in Table 1.

the three data points may be extrapolated to the Raman shift for gaseous N_2 .^{119–121} The correlation of Raman shifts with N–N bond length is consistent with the observation that the overall complex structure remains unchanged by removing either 1e or 2e from **2**: only Mo–N and N–N distances of the MoNNMo core are changed by altering the charge.

DFT and Electronic Absorption Spectroscopy. Using the experimental X-ray diffraction structures of **2** and 2^{2+} as a starting geometry, density functional theory (DFT)¹²⁴ optimized geometries were obtained for both $\mu-N_2$ complexes (see Supporting Information, Tables S2 and S3). The frontier orbitals calculated for 2^{2+} indicate that the HOMO corresponds to the bonding interaction between the Mo d orbitals and the π^* orbital of N_2 whereas the LUMO is NN π bonding in character (Figure 9). Such an analysis leads one to expect that that population of the LUMO orbitals by either 1e or 2e would enhance the bonding between the two nitrogen atoms. This interpretation is nicely supported by the X-ray and Raman data described above: upon reduction of $2[B(Ar^F)_4]_2$ to either $2[B(Ar^F)_4]$ or **2**, shortening of the N–N bond is observed by X-ray crystallography and a higher energy ν_{NN} is observed by Raman spectroscopy.

It is interesting that the LUMO+2 is a low-lying σ symmetry orbital. This orbital contains NN antibonding character but may be viewed as substantially metal-based. The LUMO+3 is a π -symmetry orbital that is NN antibonding in character. However, the metal-localized lobes in LUMO+3 are not coplanar with the nitrogen-based orbitals. Strongly antibonding π -symmetry orbitals of the MoNNMo core are actually much higher in energy (see Supporting Information for orbital energies).

This molecular orbital analysis is consistent with previous treatments.^{10,20,125–127} For example, the short N–N bond in $[(\mu-N_2)(Ru(NH_3)_5)_2][BF_4]_4$ (1.124 Å, $\nu_{NN} = 2100$ cm^{-1}) has been attributed to filled orbitals of Ru–N antibonding character.^{127–129} Accordingly, an intense absorption ($\lambda = 263$ nm, $\epsilon = 48000$

- (116) Mork, B. V.; Tilley, T. D. *J. Am. Chem. Soc.* **2004**, *126*, 4375–4385.
 (117) Hendrich, M. P.; Gunderson, W.; Behan, R. K.; Green, M. T.; Mehn, M. P.; Betley, T. A.; Lu, C. C.; Peters, J. C. *Proc. Natl. Acad. Sci. U.S.A.* **2006**, *103*, 17107–17112.
 (118) Badger, R. M. *J. Chem. Phys.* **1935**, *3*, 710–714.
 (119) Butcher, R. J.; Jones, W. J. *J. Chem. Soc., Faraday Trans.* **1974**, *70*, 560–563.
 (120) Jørgen, B. *J. Raman Spectrosc.* **1974**, *2*, 133–145.
 (121) Jones, W. J. *Can. J. Phys.* **2000**, *78*, 327–390.
 (122) Ebsworth, E. A. V.; Rankin, D. W. H.; Cradock, S. *Structural Methods in Inorganic Chemistry*; Blackwell Scientific Publications: Cambridge, MA, 1991, p 228–233.
 (123) Bersuker, I. B. *The Jahn–Teller Effect*; Cambridge University Press: New York, 2006.

- (124) Baerends, E. J.; et al. *ADF2004.01 ed. Theoretical Chemistry*; Vrije Universiteit: Amsterdam, The Netherlands, 2004; <http://www.scm.com>.
 (125) O'Regan, M. B.; Liu, A. H.; Finch, W. C.; Schrock, R. R.; Davis, W. M. *J. Am. Chem. Soc.* **1990**, *112*, 4331–4338.
 (126) Sanner, R. D.; Manriquez, J. M.; Marsh, R. E.; Bercaw, J. E. *J. Am. Chem. Soc.* **1976**, *98*, 8351–8357.
 (127) Richardson, D. E.; Sen, J. P.; Buhr, J. D.; Taube, H. *Inorg. Chem.* **1982**, *21*, 3136–3140.
 (128) Harrison, D. F.; Weissberger, E.; Taube, H. *Science* **1968**, *159*, 320–322.
 (129) Treitel, I. M.; Flood, M. T.; Marsh, R. E.; Gray, H. B. *J. Am. Chem. Soc.* **1969**, *91*, 6152–6153.

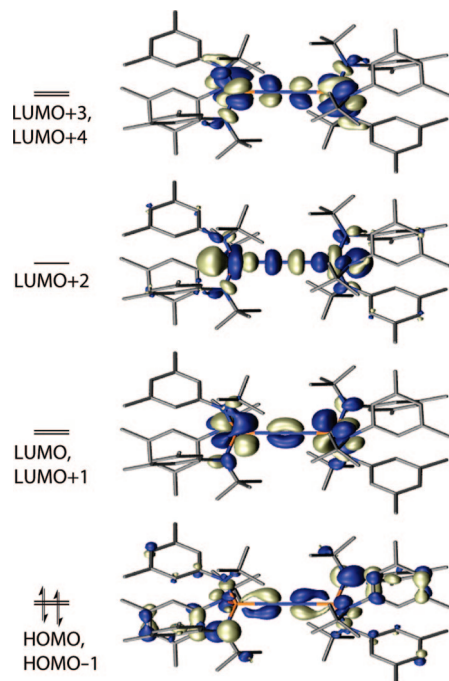


Figure 9. Selected frontier orbitals of $2[\text{B}(\text{Ar}^{\text{F}})_4]_2$ show N–N bonding character of the LUMO. Orbitals are drawn at an isosurface value of 0.037. For simplicity, only one orbital is drawn for pairs of orbitals that are close in energy and transform under the same irreducible representation in the S_6 point group. The all-bonding MoNNMo orbital is much lower in energy and not shown.

$\text{M}^{-1} \text{cm}^{-1}$) was assigned as the NN $d\pi \rightarrow \pi^*$ transition. At the time, the energy of that transition was a suggested parameter for N–N bond activation, hinting at the possibility of photochemical reactions of the MNNM core ($\text{M} =$ transition metal).¹²⁹

In view of the molecular orbital analysis presented for $2[\text{B}(\text{Ar}^{\text{F}})_4]_2$, it is of interest to examine the origin of the intense absorption band that appears in the visible region for 2 , $2[\text{B}(\text{Ar}^{\text{F}})_4]$, and $2[\text{B}(\text{Ar}^{\text{F}})_4]_2$ (Figure 5). The visible absorbance for each of the three has both similar energy and intensity: for 2 , 544 nm ($\epsilon = 41000 \text{ M}^{-1} \text{cm}^{-1}$); for $2[\text{B}(\text{Ar}^{\text{F}})_4]$, 506 nm ($\epsilon = 38000 \text{ M}^{-1} \text{cm}^{-1}$); and for $2[\text{B}(\text{Ar}^{\text{F}})_4]_2$, 510 nm ($\epsilon = 39800 \text{ M}^{-1} \text{cm}^{-1}$) (Figure S10). Considering first $2[\text{B}(\text{Ar}^{\text{F}})_4]_2$, it is expected that the intense red color of this compound arises from a suitable electronic transition that promotes $1e$ from the HOMO to one of the low-lying empty orbitals. Time-dependent DFT^{130–132} found that promoting $1e$ from the HOMO into the LUMO is a low-energy process; however, promotion of $1e$ to the LUMO+2 was predicted to have much greater intensity in the absorption spectrum. Assigning the UV–vis spectra of $2[\text{B}(\text{Ar}^{\text{F}})_4]$ and 2 is further complicated by the presence of unpaired electrons that give rise to a large number of excited-state electronic configurations. A detailed description of those electronic transitions that give rise to the observed spectra remains a topic for future detailed investigation.

Photochemistry of 2 . Recent theoretical attention has been focused on the possibility that inert, linear $\mu\text{-N}_2$ complexes might engage in photochemical reactions that productively use the N_2 fragment. One study suggested that low-lying excited states may

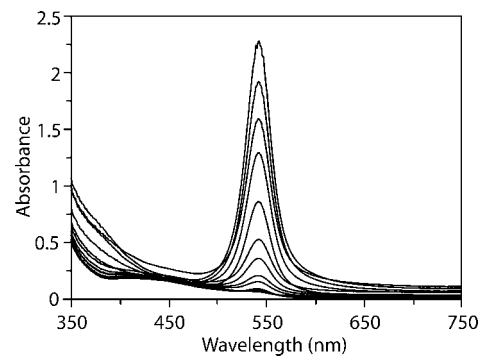


Figure 10. The UV–vis stack plot shows the bleach at 544 nm that accompanies 1-s periods of irradiation ($\lambda_{\text{irr}} = 546 \text{ nm}$) of 2 .

contain more N–N antibonding character than the ground state. These authors described a geometric distortion of the MNNM ($\text{M} = \text{Fe}, \text{Ru}$) core from a linear to a trans-bent, “diazenido-like” structure in the first singlet excited state.³⁷ We felt that this “diazenido-like” core resembled the putative zig-zag transition state, 2^\ddagger , for cleavage of the N–N bond. Having acquired a more thorough picture of the electronic structure of 2 we were compelled to explore possible photoreactions occurring from the MoNNMo core. One previously reported example of such a reaction resulted in photochemical N–N bond cleavage; irradiation of $(\mu\text{-N}_2)[\text{Mo}(\text{Mes})_3]_2$ forms $(\mu\text{-N})[\text{Mo}(\text{Mes})_3]_2$ and 0.5 equiv N_2 .³⁸

Motivated by these ideas, we explored the photochemistry of 2 when irradiated in the region of the intense, visible absorption band centered at 544 nm. To isolate this absorbance, it was convenient to use the 546 nm Hg-line of an Hg–Xe arc lamp. Irradiation of 2 in Et_2O at this wavelength results in a rapid bleach at 542 nm, accompanied by a slight increase in absorbance near 430 nm (Figure 10). Bulk photolysis of 2 was carried out using broadband light ($\lambda_{\text{irr}} \geq 480 \text{ nm}$) at -78°C , at which temperature 2 is sufficiently thermally stable to isolate the photochemical process. Treatment of 2 in this way forms a mixture of 1 and 3 in an approximate 1:1 ratio, while releasing 0.5 equiv of N_2 (Scheme 4).¹³³ This procedure was repeated with $^{15}\text{N}_2$ - 2 to unambiguously demonstrate that ^{15}N - 3 (^{15}N NMR: $\delta = 839.5 \text{ ppm}$) is formed from the $\mu\text{-N}_2$ ligand. The efficiency of the photoreaction was assayed at -78°C by both ferrioxalate and Reinicke salt actinometry.^{134–136} Both methods determined a primary quantum yield of $\Phi_{\text{p}} = 0.05$ with respect to 2 .

In an attempt to observe an intermediate in the photoreaction, the electronic transient absorption spectrum was acquired immediately following photolysis of 2 with a 544 nm, 10 ns laser pulse (Figure S12). The obtained transient absorption spectrum matched a digitally subtracted spectrum of 2 and products formed during photolysis, indicating that

(133) Following photolysis, the crude reaction mixture was treated with NO to convert paramagnetic 1 into the previously characterized, diamagnetic species $\text{ONMo}[\text{t-BuAr}]_3$. Integration of the ^1H NMR spectrum led to an observed ratio of 56:44 of nitrosyl to 3 . The loss of N_2 is assumed on the basis of the observed product distribution but not quantified.

(134) Montalti, M.; Credi, A.; Prodi, L.; Gandolfi, T. M. *Handbook of Photochemistry*; 3rd ed.; Taylor & Francis: New York, 2006; p 600–616.

(135) Hatchard, C. G.; Parker, C. A. *Proc. R. Soc. London, Ser. A* **1956**, 518–536.

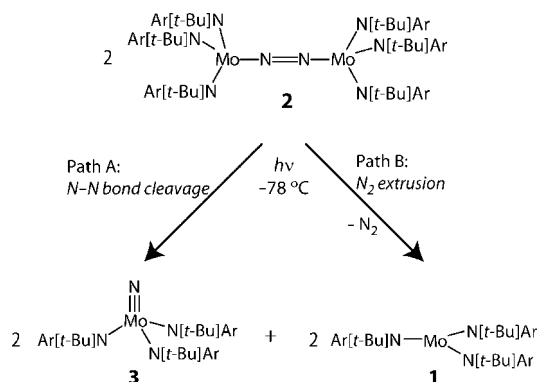
(136) Wegner, E. E.; Adamson, A. W. *J. Am. Chem. Soc.* **1966**, 88, 394–404.

(130) Kootstra, F.; Boeij, P. L. d.; Snijders, J. G. *J. Chem. Phys.* **2000**, 112, 6517–6531.

(131) Romaniello, P.; Boeij, P. L. d. *J. Chem. Phys.* **2007**, 127, 174111.

(132) Romaniello, P.; Boeij, P. L. d. *Phys. Rev. B* **2005**, 71, 155108.

Scheme 4

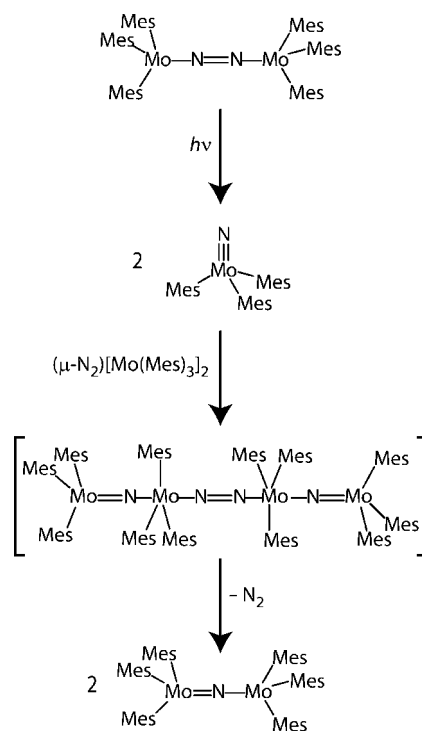


the photochemical bleach is completed within the 10 ns laser pulse. Single-wavelength kinetics, obtained by monitoring the bleach at 530 nm, agree with this result (Figure S13). These data indicate that transient absorption measurements need to be performed on a faster time scale to capture the absorption spectrum of possible intermediates in the photoreaction.

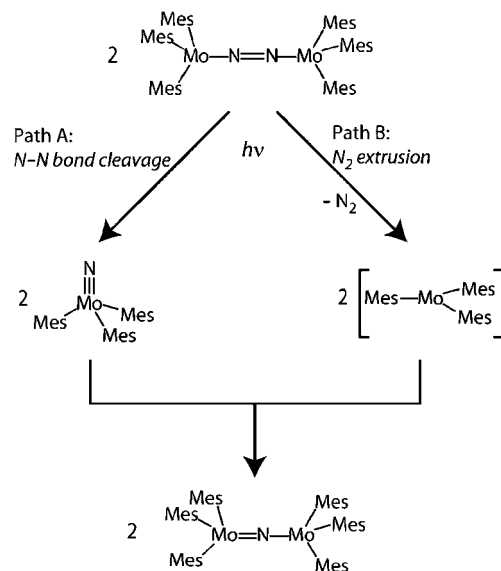
In contrast to thermal N–N bond cleavage by **2**, the photochemical fragmentation of **2** produces both **1** and **3** (Scheme 4). The observed bifurcation of the reaction path in the photoreaction of **2** is intriguing. Loss of N₂ from **2** is a process reminiscent of N₂ extrusion from organic azo complexes,^{137–140} and most likely proceeds from an electronic excited state. The other process, homolytic fragmentation of the N–N bond, resembles the thermally induced fragmentation of **2**. Currently, we are unable to distinguish whether N–N bond cleavage occurs from the electronic excited-state that is responsible for the observed visible transition or from a lower-energy state.^{141,142}

A competition between N–N bond fragmentation and N₂ extrusion, as described above for **2**, may be responsible for the isolation of (μ-N)[Mo(Mes)₃]₂ upon bulk photolysis of (μ-N₂)[Mo(Mes)₃]₂. Floriani proposed that photolysis of (μ-N₂)[Mo(Mes)₃]₂ fragments the N–N bond, and that the 2 equiv of NMo(Mes)₃ so generated are quickly trapped by (μ-N₂)[Mo(Mes)₃]₂ forming (μ-N₂)[Mo(Mes)₃NMo(Mes)₃]₂ (Scheme 5). Loss of N₂ from this putative tetramolybdenum intermediate was the favored explanation for the observed products.³⁸ An alternative mechanism is that both NMo(Mes)₃ and Mo(Mes)₃ are rapidly formed during photolysis and recombine to form (μ-N)[Mo(Mes)₃]₂ (Scheme 6). This latter mechanism agrees well with our observed product ratio obtained by bulk photolysis. The absence of a μ-nitrido product in our case is a consequence of the large kinetic barrier toward forming a μ-nitrido when bulky *tert*-butyl anilide ligands are present.^{75,143,144} In fact, we

Scheme 5



Scheme 6



have shown that **1** does not react with **3** to give a μ-nitride product due to the steric constraints.^{10,143}

Comparison Between Thermal and Photochemical N–N Bond Cleavage. A key distinction between the thermal and photochemical reactions of **2** is the observed product distribution. Upon photolysis **2** produces a mixture of **1** and **3**, whereas thermal N–N bond scission produces **3** as the sole product. This change may reflect the preference for lower energy pathways with respect to the ground-state for the thermal reaction, in contrast to photochemical processes that involve excited molecular states. For example, we have suggested that rotation of an anilide ligand may be a feature of **2**[‡], providing a means to lower the activation barrier for N–N thermal bond cleavage. However, geometric effects that stabilize the thermal

- (137) Closs, G. L.; Kaplan, L. R. *J. Am. Chem. Soc.* **1969**, *91*, 2168–2169.
 (138) Fox, J. R.; Hammond, G. S. *J. Am. Chem. Soc.* **1964**, *86*, 4031–4035.
 (139) Bartlett, P. D.; Porter, N. A. *J. Am. Chem. Soc.* **1968**, *90*, 5317–5318.
 (140) Turro, N. J. *Modern Molecular Photochemistry*; University Science Books: Sausalito, CA, 1991; p 544–550.
 (141) Kasha, M. *Discuss. Faraday Soc.* **1950**, *9*, 14–19.
 (142) Turro, N. J.; McVey, J.; Ramamurthy, V.; Lechtken, P. *Angew. Chem., Int. Ed. Engl.* **1979**, *18*, 572–586.
 (143) Johnson, M. J. A.; Lee, P. M.; Odom, A. L.; Davis, W. M.; Cummins, C. C. *Angew. Chem., Int. Ed. Engl.* **1997**, *36*, 87–91.
 (144) Stephens, F. H.; Johnson, M. J. A.; Cummins, C. C.; Kryatova, O. P.; Kryatov, S. V.; Rybak-Akimova, E. V.; McDonough, J. E.; Hoff, C. D. *J. Am. Chem. Soc.* **2005**, *127*, 15191–15200.

transition state may not be required under higher-energy photochemical conditions. Taking this view to an extreme, in the photochemical reaction the structure of the N₂ cleavage transition state might be entirely altered, as it has been shown that thermal and photochemical pathways can proceed through transition states having distinct structures due to orbital-symmetry effects.^{68,146}

Conclusions

The X-ray crystal structure of **2** had previously eluded us. Having obtained a suitable structure, we addressed a number of outstanding questions concerning the structure and magnetism of this linear, bimetallic μ -N₂ complex. Moreover, we have suggested that ligand rotation about the Mo–N_{anilide} bond may play an important role in reducing the kinetic barrier toward N–N bond cleavage by **2** under thermal conditions.

To our knowledge, no other study has directly compared X-ray crystal structures and Raman shifts of linear, bimetallic μ -N₂ complexes in three states of charge. Here, we have shown that for a series of dinitrogen-derived μ -N₂ complexes the common markers for N–N bond activation indicate that the N–N bond is activated further by removing 1e or 2e from the MoNNMo core. The reduction in N–N bonding that accompanies oxidation of **2** was rationalized by DFT studies that show N–N bonding character in the LUMO of 2[B(Ar^F)₄]₂, corresponding to the occupied HOMO of **2**.

Floriani previously reported photochemical cleavage of the N–N bond in a linear, bimetallic μ -N₂ complex to form a μ -nitrido product.³⁸ We have now demonstrated that this reaction is not unique to Floriani's system, and we have proposed a more concise, revised mechanism on the basis of our isolation of a terminal nitride product (Scheme 6). Further exploitation of this strategy for N–N bond cleavage could make for interesting future work. For instance, it is tempting to apply our finding of photochemical N–N bond scission to a number of systems (MoNNMo) that contain the requisite number of electrons for 6e cleavage but are thermally stable.^{57,147–150}

Experimental Procedures

Details concerning general remarks for handling of air-sensitive compounds, determination of molecular structure by X-ray diffraction, computational details, and procedures for photochemical reaction and physical measurements are contained in the Supporting Information document. Given here are procedures for the synthesis and isolation of **2**, 2[B(Ar^F)₄], and 2[B(Ar^F)₄]₂ alongside detailed characterization data for new compounds.

Synthetic Procedures. Preparation of (μ -N₂)[Mo(N[*t*-Bu]Ar)₃]₂(2**).**^{10,11,16} As an orange powder, Mo(N[*t*-Bu]Ar)₃ (5.081 g, 8.143 mmol) was loaded into a 250 mL Erlenmeyer flask. This solid was then dissolved in 125 mL of THF with rapid stirring. The stir bar was removed from the flask, and the flask was capped with a rubber septum. The flask was then stored at –35 °C for 10 d under N₂. The flask was removed from the freezer every 3 d to readmit N₂ into the flask. Over the first 7 d, the color of the solution became dark purple but few solids had precipitated. After 10 d, a large amount of powder had precipitated and 3.145 g of **2** was isolated by filtration of the mixture. The solids were washed with *n*-pentane (10 mL × 2). The filtrate was concentrated to 50 mL and stored at

–35 °C for an additional 7 d to afford each of the 3 additional crops (Overall, 4.760 g, 3.730 mmol, 91.6%). Purple solids were washed with MeCN, in which **2** is entirely insoluble, and dried to constant mass prior to magnetic studies: μ_{eff} (SQUID) = 2.42 μ_{B} . UV–vis (Et₂O, 20 °C): λ (ϵ) = 299 (67600), 544 (41000) nm (M^{–1} cm^{–1}).

Preparation of (μ -N₂)[Mo(N[*t*-Bu]Ar)₃]₂[B(Ar^F)₄]₂(2**[B(Ar^F)₄]₂) by Oxidation of **2**.** At –116 °C, to a rapidly stirred, blue solution of [Cp₂Fe][B(Ar^F)₄] (1.796 g, 1.712 mmol, 2 equiv) in 50 mL of Et₂O was added a solution of **2** (1.09 g, 0.856 mmol) in 40 mL of Et₂O over 2 min. The mixture became dark brown in color after approximately 25 mL of the solution of **2** has been added. The intensity of the brown color grew over the next 5 min. To the mixture was added 40 mL of thawing *n*-pentane (–130 °C) to quickly precipitate the product as a red powder. The product was then isolated by filtration. The solids were washed with *n*-pentane (30 mL × 4) and then Et₂O (20 mL × 4). Drying solids under a dynamic vacuum yields the product, 2[B(Ar^F)₄]₂ (2.530 g, 0.842 mmol, 98.4%), mp = 135–140 °C (dec). ¹H NMR (500 MHz, 20 °C, CD₂Cl₂): δ = 7.70 (16 H, s, *o*-Ar^F), 7.54 (8 H, s, *p*-Ar^F), 7.17 (6 H, s, *p*-Ar), 6.71 (6 H, s, *o*-Ar), 4.50 (6 H, s, *o*-Ar), 2.35 (18 H, s, Ar-Me), 2.17 (18 H, s, Ar-Me), 1.41 (54 H, s, *t*-Bu) ppm. ¹³C NMR (125 MHz, 20 °C, CD₂Cl₂): δ = 162.0 (q, *ipso*-Ar^F), 147.3 (s, *ipso*-Ar), 139.8 (s, Ar), 139.5 (s, Ar), 135.2 (s, *o*-Ar^F), 132.7 (s, Ar), 129.5 (q, *m*-Ar^F), 127.9 (s, Ar), 126.3 (s, Ar), 125.2 (q, CF₃), 117.9 (s, *p*-Ar^F), 74.0 (s, CMe₃), 31.5 (s, NCCH₃), 22.2 (s, Ar-CH₃), 21.4 (s, Ar-CH₃) ppm. ¹⁹F NMR δ = (376 MHz, 20 °C, CD₂Cl₂): δ = –63 ppm. UV–vis (CH₂Cl₂, 20 °C): λ (ϵ) = 296 (79200), 382 (30600), 514 (39800) nm (M^{–1} cm^{–1}). Anal. Calcd for C₁₃₆H₁₃₂B₂F₄₈Mo₂N₈: C, 54.38; H, 4.43; N, 3.73; F, 30.36. Found: C, 54.02; H, 4.34; N, 3.66; F, 30.22.

The ¹⁵N labeled derivative was prepared in an analogous fashion from ¹⁵N-labeled **2**.¹⁰ For ¹⁵N-labeled 2[B(Ar^F)₄]₂, ESI-MS: *m/z* (calcd, assignment) = 640.3426 (640.3423, 2²⁺), 1222.6277 (1222.6069, [2-(*t*-Bu)]⁺, 1279.6773 (1279.6907, 2⁺).

Preparation of (μ -N₂)[Mo(N[*t*-Bu]Ar)₃]₂[B(Ar^F)₄]₂(2**[B(Ar^F)₄]₂) by Comproportionation of **2** and 2[B(Ar^F)₄].** To a red solution of 2[B(Ar^F)₄]₂ (1.500 g, 0.500 mmol) in 25 mL of THF was added **2** (700 mg, 0.548 mmol, 1.1 equiv) as a purple solid at 20 °C. Upon mixing the purple **2** with the opaque, red solution of 2[B(Ar^F)₄]₂, a cranberry-colored solution formed. The vial containing **2** was rinsed with 10 mL of THF which was added to the stirring solution. Once the addition was completed, the solution was allowed to stir for 1 min before the solvent was removed under a dynamic vacuum. The remaining solids were then scraped onto a sintered glass frit and thoroughly washed with toluene (20 mL × 5) to remove a pale yellow solution (presumably containing **3**) and then the remaining solids were washed with *n*-pentane (20 mL × 4) before the solids were dried under a dynamic vacuum. The cranberry-colored solids of 2[B(Ar^F)₄]₂ were then collected (2.030 g, 0.948 mmol, 95.0%), mp 140–142 °C (dec). ¹H NMR (500 MHz, 20 °C, CDCl₃): δ = 7.70 (8 H, s, $\Delta\nu_{1/2}$ = 9.7 Hz, *o*-Ar^F), 7.51 (4 H, s, $\Delta\nu_{1/2}$ = 5.2 Hz, *p*-Ar^F), 6.08 (27 H, s, $\Delta\nu_{1/2}$ = 75 Hz, *t*-Bu), 5.47 (6 H, s, $\Delta\nu_{1/2}$ = 72 Hz, *o*-Ar), 1.25 (3 H, s, $\Delta\nu_{1/2}$ = 6.8 Hz, *p*-Ar), 1.74 (18 H, s, $\Delta\nu_{1/2}$ = 14.5 Hz, Ar-Me) ppm. μ_{eff} (SQUID) = 1.96 μ_{B} . UV–vis (CH₂Cl₂, 20 °C): λ (ϵ) = 295 (63800), 508 (38000) nm (M^{–1} cm^{–1}). Anal. Calcd for C₁₀₄H₁₂₀BF₂₄Mo₂N₈: C, 58.35; H, 5.64; N, 5.23; F, 21.30. Found: C, 58.64; H, 5.66; N, 5.05; F, 20.91.

Acknowledgment. This paper is dedicated to the memory of Professor Carlo Floriani. Emily Nytko-Lutz and Dr. Dino Villagrán are thanked for assistance with the acquisition of

(145) These two energies may be compared in cm^{–1} at 293 K: $k_{\text{B}}T$ is 207 cm^{–1} in comparison to 18382 cm^{–1} for 544 nm.

(146) Woodward, R. B.; Hoffmann, R. *J. Am. Chem. Soc.* **1965**, *87*, 395–397.

(147) Ferguson, R.; Solari, E.; Floriani, C.; Osella, D.; Ravera, M.; Re, N.; Chiesi-Villa, A.; Rizzoli, C. *J. Am. Chem. Soc.* **1997**, *119*, 10104–10115.

(148) O'Donoghue, M. B.; Zanetti, N. C.; Davis, W. M.; Schrock, R. R. *J. Am. Chem. Soc.* **1997**, *119*, 2753–2754.

magnetic data. We are indebted to Dr. Eckhard Bill and Prof. Karsten Meyer for stimulating discussions and for suggesting a suitable magnetic model for **2**. Dr. Eckhard Bill is also thanked for making available his wonderful julX program. We are grateful to Professors Daniel G. Nocera, Andrei Tokmakoff, and Troy Van Voorhis for helpful discussions. We acknowledge Tim McClure for making available the Raman spectroscopy instrumentation in the Center for Materials Science and Engineering. We gratefully thank the NSF for funding this work (Grant CHE-719157).

(149) Greco, G. E.; Schrock, R. R. *Inorg. Chem.* **2001**, *40*, 3850–3860.

Note Added after ASAP Publication. The version of this paper published on June 25, 2008, contained an error on page 9401. The N–N distance has been corrected to 1.138(6) Å. The version published on July 16, 2008 has the correct information.

Supporting Information Available: Complete ref 124; full experimental details and cif files. This material is available free of charge via the Internet at <http://pubs.acs.org>.

JA8002638

(150) Greco, G. E.; O'Donoghue, M. B.; Seidel, S. W.; Davis, W. M.; Schrock, R. R. *Organometallics* **2000**, *19*, 1132–1149.